





RAPID COMMUNICATION

Multiple coordinated cellular dynamics mediate CA1 map plasticity

Kotaro Mizuta^{1,2}  | Junichi Nakai^{3,4,5}  | Yasunori Hayashi^{1,2,4}  | Masaaki Sato^{2,3,4,6,7} ¹Department of Pharmacology, Kyoto University Graduate School of Medicine, Kyoto, Japan²RIKEN Brain Science Institute, Wako, Saitama, Japan³Graduate School of Science and Engineering, Saitama University, Saitama, Japan⁴Brain and Body System Science Institute, Saitama University, Saitama, Japan⁵Division of Oral Physiology, Tohoku University Graduate School of Dentistry, Sendai, Miyagi, Japan⁶RIKEN Center for Brain Science, Wako, Saitama, Japan⁷Department of Neuropharmacology, Hokkaido University Graduate School of Medicine, Sapporo, Hokkaido, Japan**Correspondence**Masaaki Sato, Department of Neuropharmacology, Hokkaido University Graduate School of Medicine, Sapporo, Hokkaido 060-8638, Japan.
Email: msato@pop.med.hokudai.ac.jp**Funding information**

Japan Agency for Medical Research and Development, Grant/Award Number: Program for Brain Mapping by Integrated Neurotechn; Japan Science and Technology Agency, Grant/Award Number: JPMJPR12A1; Japan Society for the Promotion of Science, Grant/Award Numbers: 15H01571, 15H05723, 16H01292, 16H06536, 17H05695, 17H05985, 17K19633, 18H05434, 19H04942, 19K16293, 20H03550, 20K21561, 22110006, 25830023, 26115504; Ministry of Education, Culture, Sports, Science and Technology, Grant/Award Number: Regional Innovation Cluster Program grant; RIKEN

Abstract

In the hippocampus, spatial and nonspatial information are jointly represented as a neural map in which locations associated with salient features are over-represented by increased densities of relevant place cells. Although we recently demonstrated that experience-dependent establishment of these disproportionate maps is governed by selective stabilization of salient place cells following their conversion from non-place cells, the underlying mechanism for pre-established map reorganization remained to be understood. To this end, we investigated the changes in CA1 functional cellular maps imaged using two-photon calcium imaging in mice performing a reward-rearrangement task in virtual reality. Mice were pre-trained on a virtual linear track with a visual landmark and a reward in two distinct locations. Then, they were re-trained on the same track with the exception that the location of reward was shifted to match the landmark location. We found that, in contrast to de novo map formation, robust map reorganization occurred through parallel coordination of new place field formation, lateral shifting of existing place fields, and selective stabilization of place fields encoding salient locations. Our findings demonstrate that intricate interplay between multiple forms of cellular dynamics enables rapid updating of information stored in hippocampal maps.

KEYWORDS

calcium imaging, cognitive map, navigation, spatial memory, virtual reality

This is an open access article under the terms of the Creative Commons Attribution-NonCommercial License, which permits use, distribution and reproduction in any medium, provided the original work is properly cited and is not used for commercial purposes.

© 2021 The Authors. *Hippocampus* published by Wiley Periodicals LLC.

1 | MAIN BODY

It is well-established that locations associated with behaviorally relevant salient features, such as reward, safety, and local cues, are over-represented by a disproportionately large number of place cells (PCs) in the hippocampus (Bourboulou et al., 2019; Dupret, O'Neill, Pleydell-Bouverie, & Csicsvari, 2010; Gauthier & Tank, 2018; Hetherington & Shapiro, 1997; Hollup, Molden, Donnett, Moser, & Moser, 2001; O'Keefe & Conway, 1978; Sato et al., 2020; Wiener, Paul, & Eichenbaum, 1989; Zaremba et al., 2017). Recently, we

demonstrated that de novo establishment of these disproportionate maps involves the selective stabilization of PCs that encode salient locations following their conversion from non-PCs (Sato et al., 2020). However, the cellular dynamics underlying the plasticity of pre-established maps remained unknown. Thus, we investigated changes in CA1 functional cellular maps imaged using two-photon calcium imaging in mice performing a reward-rearrangement task in virtual reality (see Detailed Methods).

We pre-trained mice on a virtual linear track where a visual landmark and a reward were placed in two distinct locations. Then, we re-

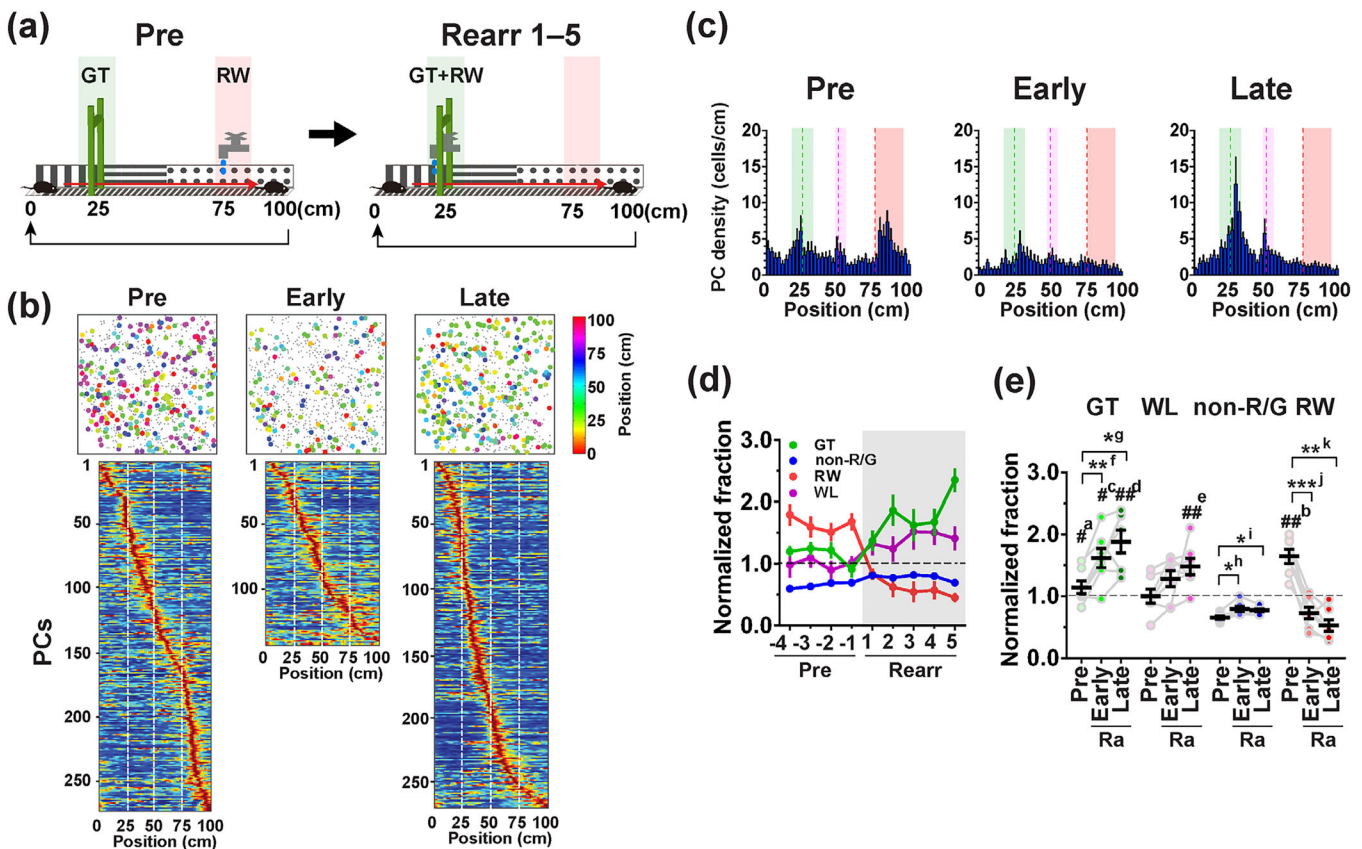


FIGURE 1 Reorganization of CA1 maps induced by conjunction of reward and landmark. (a) Design of the reward-rearrangement task. Mice were first trained on the standard linear track, which included a visual landmark (GT) and reward delivery (RW) at separate locations, in preceding control sessions (Pre, left). Once training was complete, the location of reward delivery was shifted to match the location of the landmark (GT + RW), and mice were re-trained in this new arrangement for the following five sessions (Rearr 1–5, right). (b) Examples of place cell (PC) maps imaged in the same animal in the preceding control (session Pre –1), early (session Rearr 1) and late (session Rearr 5) phases of the reward-rearrangement task (top). PCs and non-PCs are represented by filled circles of various colors and by gray dots, respectively. The different colors of filled circles represent different locations of the place fields. Heat maps shown below are the distributions of place fields in the corresponding sessions ordered by their positions (bottom). (c) Histograms indicating the distribution of PCs with respect to track position for the preceding control (session Pre –2), early (session Rearr 1) and late (session Rearr 5) phases of the rearrangement task. The average data from seven mice are presented. The green, red, and magenta dashed lines delineate the positions of the landmark, reward delivery, and boundary between different wall patterns, respectively. Areas shown in green, red, and magenta define GT, RW, and wall (WL) cells, respectively. (d) Hippocampal spatial representations expressed as the fractions of GT (green), non-R/G (blue), RW (red), and WL (magenta) cells relative to the number of total PCs identified in each session. Values were normalized relative to a uniform distribution (i.e., 0.0125/bin), and values >1 indicated over-represented locations. The periods during which the reward delivery was relocated are shaded in gray. (e) Average normalized fractions of GT (green), WL (magenta), non-R/G (blue), and RW (red) cells for the preceding control, early, and late phases of the reward-rearrangement (Ra) task. The data for “Pre” represent the average of the Pre –4, –3, –2 and –1 sessions. #^a, $p = .021$ versus non-R/G Pre, ##^b, $p = .0013$ versus non-R/G Pre, $F_{(1.419,8.511)} = 15.5$; #^c, $p = .026$ versus non-R/G Early, $F_{(1.997,11.98)} = 12.7$; ##^d, $p = .0089$ versus non-R/G Late, ##^e, $p = .0089$ versus non-R/G Late, $F_{(1.702,10.21)} = 19.8$; **f, $p = .0070$, *g, $p = .018$, $F_{(1.411,8.467)} = 10.8$; *h, $p = .024$, *i, $p = .010$, $F_{(1.489,8.932)} = 10.9$; ***j, $p = .0007$, **k, $p = .0011$, $F_{(1.413,8.480)} = 38.3$; one-way ANOVA, $n = 7$ mice [Color figure can be viewed at [wileyonlinelibrary.com](https://onlinelibrary.com)]

trained mice on the same track, but we shifted the reward location to match the landmark location (Figure 1a). The re-training period after reward rearrangement was divided into early (sessions 1–2) and late (sessions 3–5) sessions. There were no significant differences in distance traveled, average running speed, and fraction of time spent running before and after the reward was rearranged (Figure S1a). Anticipatory slowdown began to emerge before the new reward location in the late sessions (Figure S1b–c). However, robust CA1 map reorganization occurred immediately after reward rearrangement (Figure 1b). Notably, the fraction of PCs decreased immediately but recovered as re-training progressed (Figures 1b and S1d). Furthermore, over-representation of the previous reward (RW) location suddenly disappeared as early as the first rearrangement session, whereas over-representation of the location associated with the pre-existing landmark gate (GT) and the relocated reward was markedly enhanced over the course of re-training (Figure 1c–e). The effect of this enhanced over-representation was approximately additive (normalized fractions of PCs: Pre-GT, 1.14 ± 0.10 [i.e., $14 \pm 10\%$ increase compared with uniform distribution; see Figure 1d legend]; Pre-RW, 1.65 ± 0.09 [$65 \pm 9\%$ increase]; and Late GT + RW, 1.89 ± 0.18 [$89 \pm 18\%$ increase]), suggesting that the magnitude of increases in PC fractions represents the degree of salience in the hippocampal map. Notably, reward rearrangement also enhanced representation of the location associated with the wall-pattern transition (Figure 1c–e), suggesting that a salience conjunction can also be formed more broadly with nearby less salient visual cues.

By conducting a cell-by-cell comparison of maps imaged in adjacent sessions, we found that hippocampal map stability is tightly regulated in a salience-dependent, location-specific manner (Figure 2). Before reward rearrangement, place-field stability of the reward location and the landmark location was significantly higher than that of non-salient locations (Figure 2a,d; Sato et al., 2020). Reward rearrangement triggered a significant reduction in place-field stability of the previous reward location and non-salient locations in early phase re-training (Figure 2b,d). The stability of the location with conjunctive salience appeared to be maintained, although the absolute number of stable PCs markedly decreased compared with that in the original arrangement (Figure 2a–b,d). Although the stability of the non-salient locations appeared to recover in the late phase, the stability of the previous reward location remained low (Figure 2d). Overall, these results demonstrate that hippocampal map plasticity accompanies redistribution of PC stability through a short period of heightened map instability. The presence and absence of salience thus govern hippocampal map representations through dynamic regulation of place-field stability.

Next, to elucidate the cellular mechanisms underlying the map plasticity, we analyzed functional transitions of individual cells between consecutive sessions (Figures 3,4,5, S2, and S3; Sato et al., 2020). In this analysis, we first identified a population of common cells that belonged to the cell category of interest in the reference session of the two sessions compared and then tracked the position of the place field of each cell in the other session (see Detailed Methods and figure legends). Figure 3 shows the density

distributions of PCs that were derived from, or converted into, different cell categories at different phases of plasticity. For simplicity, the terms we used to categorize cells were based on the condition before reward rearrangement. Specifically, the labels “GT cells” and “RW cells” refer to PCs that encode the landmark (GT) and reward (RW) locations before reward rearrangement (Figure S2). After reward rearrangement, the field positions maintain these same designations when associated with the landmark plus reward (GT) and no salience (RW). The reward rearrangement elicited a rapid and sustained reduction in RW cell formation from non-PCs in the early and late phases and a delayed increase in GT cell formation in late phase re-training (Figures 3a and 4a). The elimination of RW cells by conversion to non-PCs subsided in the late phase (Figures 3b and 4b), which likely reflected the substantial reduction in RW cell formation in the preceding early phase. Consequently, the net effect was a remarkable transient decrease in RW cell formation in the early phase with a delayed increase in GT cell formation (Figures 3c and 4c). These results demonstrate that reward rearrangement and formation of conjunctive salience markedly influences net PC formation. Additionally, the salience-dependent down-regulation and up-regulation of PC formation underlie the rapid decrease in PC fraction and the disappearance of over-representation of the previous reward location in the early phase, as well as the recovery of the PC fraction and enhancement of over-representation of the GT location in the late phase of plasticity.

Reward rearrangement significantly increased the recruitment of GT cells from non-RW, non-GT PCs (non-R/G cells) toward the late phase of re-training (Figures 3d, 4d and 5a). Furthermore, there was a significant transient increase in recruitment of GT cells from RW cells in the early phase of re-training (Figures 3f, 4f, and 5b). These results indicate that salience conjunction augments recruitment of PCs that encode a previously salient location as well as non-salient locations. The density of stable RW cells exhibited a sudden and prolonged drop in the early and late phases (Figures 3f and 4f), whereas the density of stable GT cells remained high (Figures 3e, 4e, and 5c), consistent with our earlier findings (Figure 2). In summary, reward rearrangement-induced map reorganization is mediated by a rapid disappearance of the over-representation of the previously salient location followed by a gradual enhancement of the over-representation of the location associated with a newly formed strong conjunction of salience. In contrast to the primary role of selective place-field stabilization in initial map establishment, adaptive changes in the hippocampal salience map are cooperatively achieved by parallel engagement of multiple forms of cellular dynamics that incorporate not only stabilization but also formation and lateral shifting of place fields (Figure 6).

The observed contrast in cellular dynamics between map formation and plasticity highlights a transition between two distinct modes in hippocampal circuits during different experiences. During initial map formation, the “encoding” mode is governed by a simple formation-stabilization principle (Figure 6a; Sato et al., 2020). Upon rearrangement of salient features, the process shifts dynamically to an “updating” mode (Figure 6b). The balanced formation and disappearance of PCs, which are transiently disequibrated during early phase map plasticity, cause a rapid shift in peak PC density. Simultaneously,

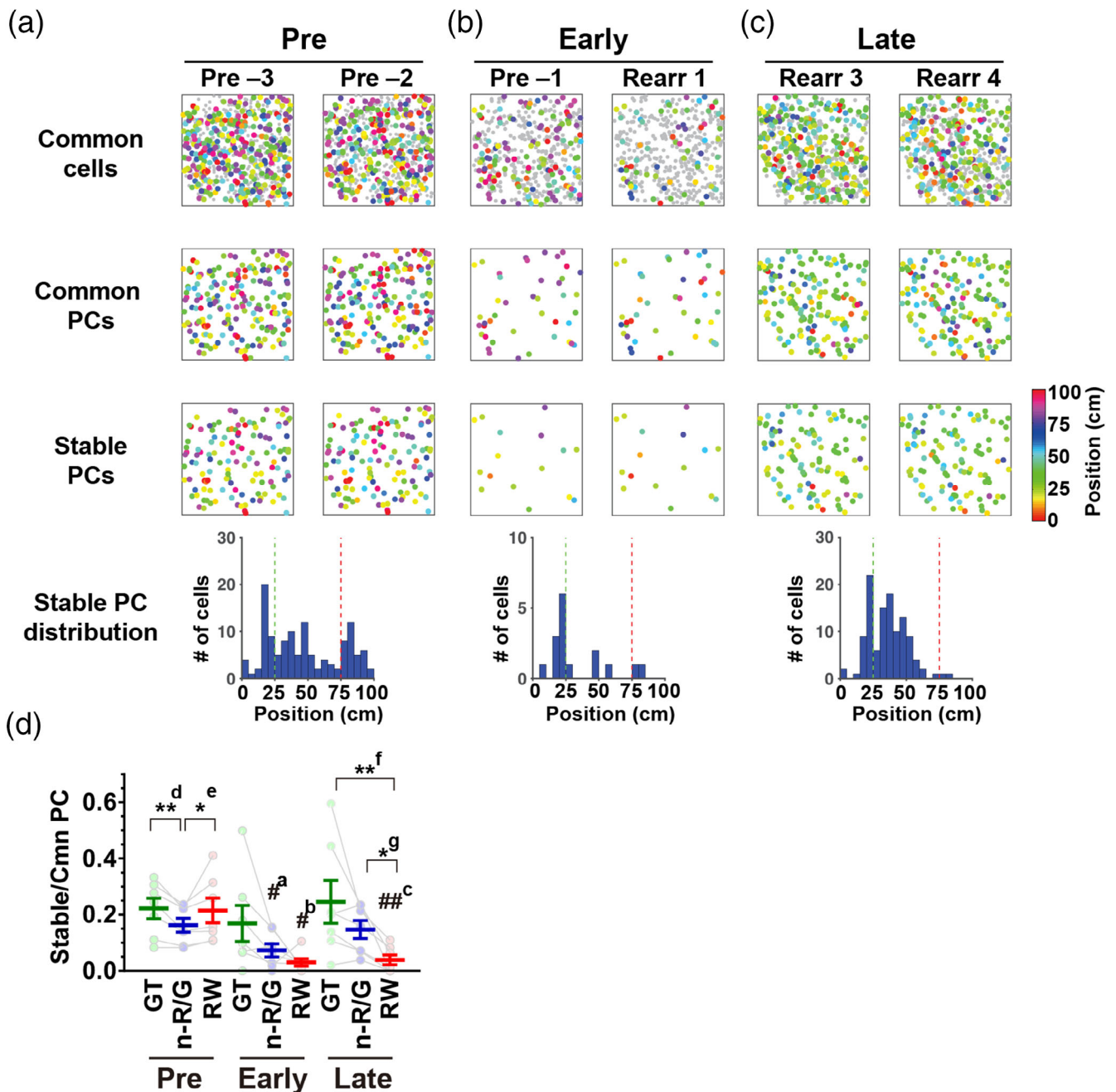


FIGURE 2 PC stability during the reward-rearrangement task. (a) Example PC maps imaged in two consecutive sessions in the preceding control phase of the reward-rearrangement task. Top, middle, and bottom maps present cells identified in common between the two sessions (Common cells), cells identified as PCs in both sessions (Common PCs), and cells identified as PCs with stable place fields in both sessions (Stable PCs), respectively. The histogram shown at the bottom indicates distributions of the stable PCs against track position. The green and red dashed lines delineate the positions of the landmark and reward delivery, respectively. The same convention applies to (b) and (c). (b–c) Example PC maps imaged in the early (b) and late (c) phases of the reward-rearrangement task in the same animal as presented in (a). Note that the Y-axis scale of the histogram shown at the bottom of (b) is different from those in (a) and (c). (d) The average PC stability for GT, non-R/G (n-R/G), and RW cells for the preceding control, early, and late phases of the reward-rearrangement task. #^a, $p = .023$ versus non-R/G Pre, $\chi^2_{(2)} = 7.14$; #^b, $p = .033$ versus RW Pre, ##^c, $p = .0063$ versus RW Pre, $\chi^2_{(2)} = 11.2$; **d, $p = .0099$, *e, $p = .023$, $\chi^2_{(2)} = 10.6$; **f, $p = .0040$, *g, $p = .049$, $\chi^2_{(2)} = 11.1$; Friedman test, $n = 7$ mice [Color figure can be viewed at wileyonlinelibrary.com]

a subset of cells that encode salient locations rapidly move their fields to locations in which salience is relocated during the early phase (Gauthier & Tank, 2018; Kobayashi, Nishijo, Fukuda, Bures, &

Ono, 1997). This process is followed by further recruitment of non-salient PCs during the late phase, which could occur via “overwriting” of pre-existing non-salient place fields by strong salience signals

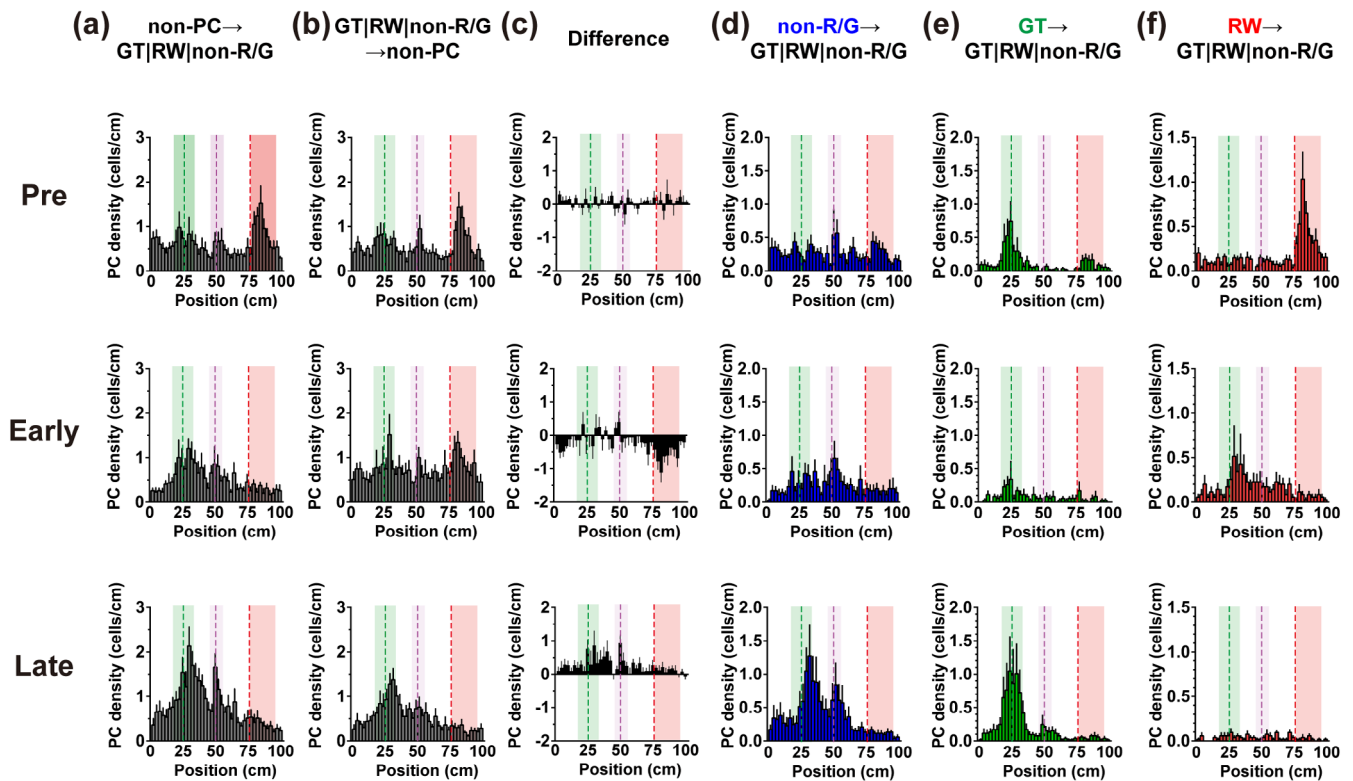


FIGURE 3 Distributions of PCs derived from, or converted into, different cell categories during map plasticity. (a) Formation of different PC categories from non-PCs. The histograms show the distributions of PCs against the track position after they were converted from non-PCs, and those for the preceding control, early and late phases of the reward-rearrangement task are shown from top to bottom. Values were averaged across all relevant comparisons of sessions (see Detailed Methods) and further averaged across all mice ($n = 7$ mice). The green, red, and magenta dashed lines delineate the positions of the landmark, reward delivery, and boundary between different wall patterns, respectively. The areas shown in green, red and magenta define GT, RW, and WL cells, respectively. (b) Elimination of different PC categories by conversion to non-PCs. The histograms show the distributions of PCs against track position before they were converted into non-PCs. (c) Net PC formation. The histograms were obtained by subtracting the histograms in (b) from the corresponding histograms in (a). (d) Transition and stability of non-R/G cells. The histograms show the distributions of PCs that were non-R/G cells in the previous sessions against the track position. (e) Transition and stability of GT cells. The histograms show the distributions of PCs that were GT cells in the previous sessions against the track position. (f) Transition and stability of RW cells. The histograms show the distributions of PCs that were RW cells in the previous sessions against the track position [Color figure can be viewed at wileyonlinelibrary.com]

derived from conjunction of multiple salient features. These remodeling processes are accompanied by the transient weakening of place-field stability during the early phase and its recovery during the late phase.

Our current results and a similar calcium imaging study illustrate the multiplicity of PC dynamics. Zaremba et al. (2017) observed PC enrichment at a reward location only after the reward was moved to a new location and they did not observe PC enrichment at cue locations. Differences between their findings and ours could be due to variations in cue richness between their treadmill belt and our virtual linear track. The increased saliency of the landmark and reward in our simpler environment likely contributed to the emergence of overrepresentation when the mice first became familiarized with the novel environment. Despite these differences, lateral shifting of non-salient place fields toward new reward locations was observed in both their study and ours (Figures 3d, 4d, and 5a), suggesting the generality of this process in map reorganization.

The results of our previous and current studies demonstrate that CA1 maps are initially highly dynamic in a manner reminiscent of global remapping and are gradually consolidated with experience and learning, so that the representations of salient locations are more strongly stabilized than those of other locations (Sato et al., 2020). This finding supports the view that hippocampal CA1 maps gradually change over time (Mankin et al., 2012; Rubin, Geva, Sheintuch, & Ziv, 2015; Ziv et al., 2013) but stands in contrast to the observation that each cell has a stable place field, while its participation in long-term population codes is highly dynamic in a manner reminiscent of rate remapping (Ziv et al., 2013). Our findings suggest that the turnover of hippocampal spatial representations is heterogeneous within a single map and can be regulated by the presence of salience. Since it was reported that the stability of place fields differs along the hippocampal trisynaptic circuit (Hainmueller & Bartos, 2018), the within-map regulation of representational stability in CA1 may act as a filter, through which the information stably coded in the dentate gyrus is

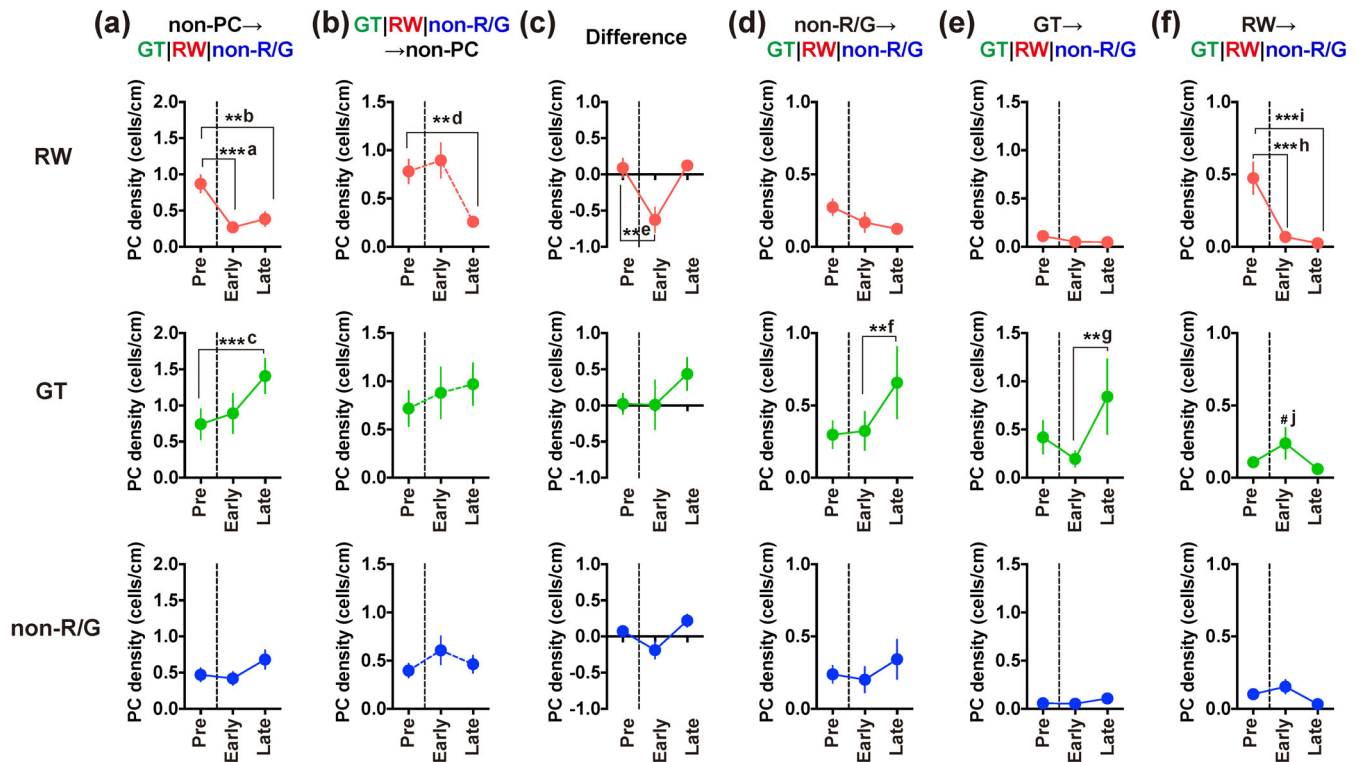


FIGURE 4 Summary data for the dynamics of each cell category during map plasticity. (a) Formation of different PC categories from non-PCs. The average cell densities of RW cells (top), GT cells (middle) and non-R/G cells (bottom) formed from non-PCs are shown for the preceding control, early, and late phases of the reward-rearrangement task. Each data point represents an average value of the cell densities across the spatial bins that correspond to the cell category of interest at that phase. The vertical dashed lines indicate the occurrence of reward rearrangement. *****a**, $p = .0005$, ****b**, $p = .0041$, *****c**, $p = .0002$, $F_{(2,12)} = 12.4$, two-way ANOVA, $n = 7$ mice. (b) Elimination of different PC categories by conversion to non-PCs. The connecting lines in these plots are represented as dashed lines to indicate that they represent the disappearance of PCs. ****d**, $p = .0041$, $F_{(2,12)} = 7.16$, two-way ANOVA, $n = 7$ mice. (c) Net PC formation. Differences between the formation and elimination of each PC subcategory are shown. ****e**, $p = .0044$, $F_{(2,12)} = 15.0$, two-way ANOVA, $n = 7$ mice. (d) Transition and stability of non-R/G cells. ****f**, $p = .0021$, $F_{(2,12)} = 5.12$, two-way ANOVA, $n = 7$ mice. (e) Transition and stability of GT cells. ****g**, $p = .0042$, $F_{(2,12)} = 7.33$, two-way ANOVA, $n = 7$ mice. (f) Transition and stability of RW cells. *****h**, $p < .0001$, *****i**, $p < .0001$, $F_{(2,12)} = 6.60$, **#j**, $p = .043$ versus Early RW, $F_{(2,12)} = 4.35$, two-way ANOVA, $n = 7$ mice [Color figure can be viewed at wileyonlinelibrary.com]

effectively transmitted to downstream subicular and entorhinal neurons.

In conclusion, the results of our previous and current studies collectively indicate that while the formation-stabilization principle governs initial map establishment, parallel and coordinated engagement of multiple forms of cellular dynamics controls adaptive reorganization of pre-established maps. This intricate interplay enables rapid updating of hippocampal cognitive maps and may provide a mechanism through which the experience of salient features forms lasting and adaptable memory traces.

2 | DETAILED METHODS

All experiments were conducted in accordance with institutional guidelines and protocols approved by the RIKEN Animal Experiments Committee. Two-photon calcium imaging of dorsal hippocampal CA1 neurons and analyses of behavioral and imaging data were conducted

as described previously (Sato et al., 2020). Briefly, adult male Thy1-G-CaMP7 transgenic mice (12 weeks old or older and weighing 28–35 g) were implanted with a hippocampal imaging window and trained on a virtual linear track (100 cm long) created in a head-fixed virtual environment (Sato et al., 2017). Different patterns were placed on the walls as follows: vertical white and black stripes (0–25 cm), horizontal white and black stripes at 25–50 cm, and black dots on a white background at 50–100 cm. Each mouse ran along it unidirectionally, and when it reached the other end of the segment, the virtual position was transferred back immediately to the origin so that the same track segment was presented again. A green gate as a visual landmark was placed 25 cm from the origin. Water rewards were provided when the mouse passed 75 cm from the origin. Mice were pre-trained on this standard track for a total of 15 sessions with 1–2 sessions per day. Then, the mice were further trained for the following five sessions (Rearrangements 1–5) in the same track, but the location of reward delivery was shifted to match the location of the landmark. Data obtained from the last four sessions of the initial 15 training sessions

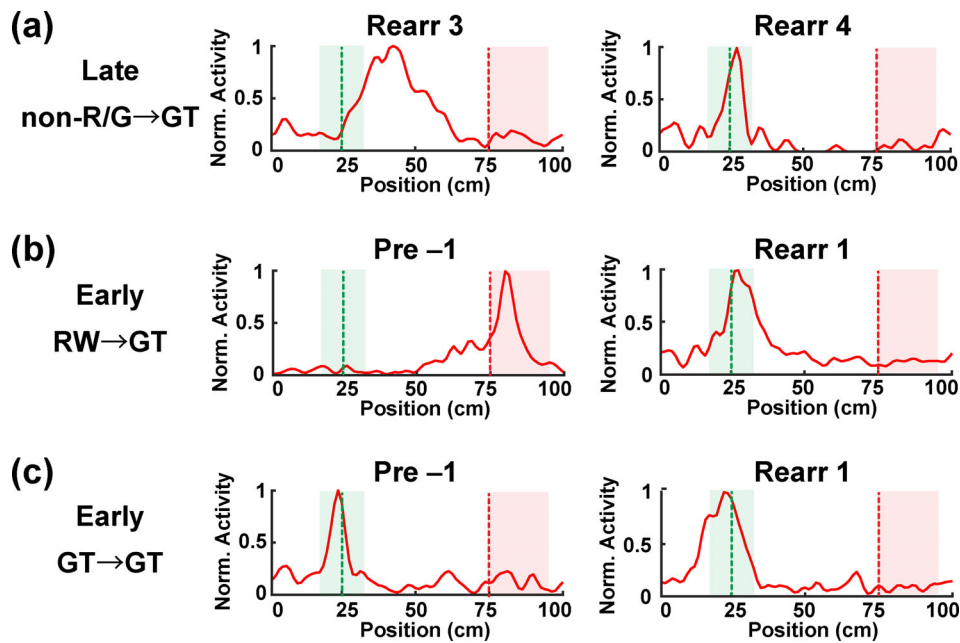


FIGURE 5 Examples of place-field changes during map plasticity. (a) Spatial tuning curves of a non-R/G cell that shifted its place field toward the reward plus landmark location in the late phase of map plasticity (Late non-R/G→GT). Tuning curves were obtained by Gaussian fitting scaled to an activity versus location histogram of the cell (see Figure S2 for examples); the curves of the two consecutive sessions being compared are shown side by side. The green and red dashed lines delineate the positions of the landmark and the reward delivery before the reward rearrangement, respectively. Areas shown in green and red define GT cells and RW cells, respectively. (b) Spatial tuning curves of a RW cell that shifted its place field to the new reward location immediately after reward relocation (Early RW→GT). (c) Spatial tuning curves of a GT cell that had a stable place field at the landmark location regardless of the reward relocation (Early GT→GT) [Color figure can be viewed at wileyonlinelibrary.com]

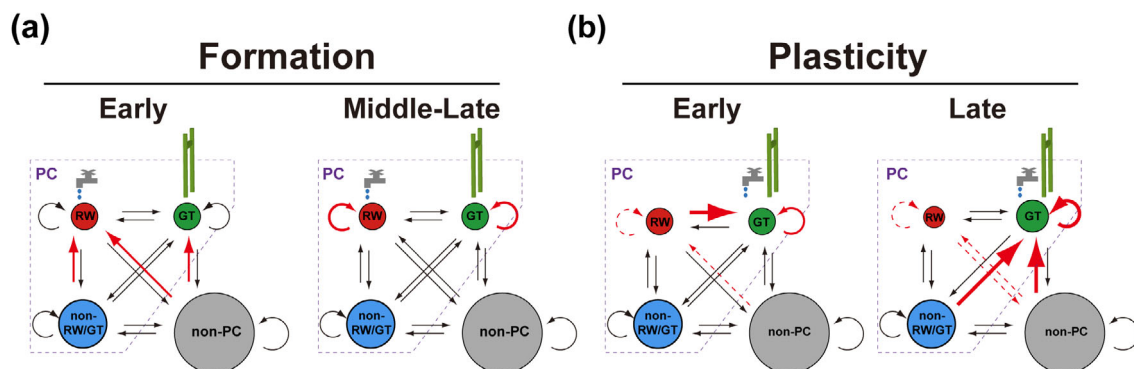


FIGURE 6 A model for the formation and plasticity of the hippocampal CA1 salience map. (a) During the early phase of formation, a seed map is laid out mainly by de novo formation of new PCs (Early). Selective consolidation of GT cells and RW cells then takes over the establishment and maintenance of the map during the middle and late phases (Middle-Late). (b) Immediately after reward rearrangement, the fraction of PCs decreases because of decreased RW cell formation and stabilization, and a subpopulation of RW cells move their fields to the new reward location (Early). After a few sessions, the stability and formation of GT cells increases, as does recruitment from non-RW/GT cells to GT cells (Late). The diagrams in panel (a) are reproduced for comparison from Sato et al. (2020). The processes shown in red are the key processes in each phase, which are based on the data in Sato et al. (2020) and Figure 4. Augmentation and reduction of the processes during plasticity are depicted by thickened and dashed lines, respectively [Color figure can be viewed at wileyonlinelibrary.com]

(referred to as Pre -4 through -1) were analyzed as preceding control sessions. We conducted the first rearrangement sessions immediately following the last preceding control sessions without releasing the mice from head fixation. Slowdown of running speed before the

reward point was calculated as the difference between the average running speed in the zone immediately before (0-10 cm) the reward point and the maximum average running speed in the area 0-30 cm before that zone. While mice performed the behavioral task,

fluorescence of G-CaMP7 and coexpressed DsRed2 in hippocampal CA1 pyramidal neurons was imaged at a rate of 15 frames per second using a Nikon A1MP (Nikon, Tokyo, Japan) equipped with a 16 \times , NA 0.8 water immersion objective lens (CFI75 LWD 16 \times W, Nikon). G-CaMP7 and DsRed2 were excited at 910 nm using a Ti-sapphire laser (Mai Tai DeepSee eHP, Spectra-Physics, Santa Clara, CA).

Cell morphology and activity time-series were computationally extracted from G-CaMP7 movies using a modified nonnegative matrix factorization as previously described (Sato et al., 2020). Place fields were calculated using cellular activity during movement periods (at a speed >0.5 cm/s continuously for a duration >2 s). Statistical significance of place-related activity was tested by calculating the mutual information content between neuronal activity and the mouse's virtual location for each cell and comparing this value to a distribution of mutual information content calculated using 1,000 randomly permuted data for the same cell. Cells were considered PCs if their overall activity rates within the session were no less than 0.1 events/s and their mutual information content in the real data was greater than the 95th percentile of values obtained from the randomly permuted data. The position of the place field of each PC was defined by the position of its peak. A PC was considered a "gate (GT) cell," "reward (RW) cell," or "wall (WL) cell" if the position of its place field was 17.5–32.5, 75–95, or 47.5–55 cm, respectively, from the track segment origin. PCs with place fields outside the above zones were categorized as non-reward, non-gate PCs (non-R/G cells).

Cell imaged in different sessions were registered by two-dimensional correlation-based map alignment followed by centroid distance-based cell identification as previously described (Sato et al., 2020). In our analysis, we found that the quality of the image alignment was gradually reduced as the number of sessions that separated the two images increased (Sato et al., 2020). Therefore, we conservatively focused on the comparisons between two consecutive sessions. Common PCs were defined as cells that were identified as significant PCs in both consecutive sessions. Stable PCs were defined as a subset of common PCs with place-field positions in the consecutive sessions that were close to each other (i.e., place-field distance <10 cm). In the analysis of cellular transitions, we first identified a population of common cells that belonged to the cell category of interest in the reference session N and then tracked the position of the place field of each cell in the subsequent session N + 1, except for the elimination of PCs to non-PCs (Figures 3b and 4b), for which we instead analyzed the position of the place fields in session N. In Figures 3, 4, and S3, data for "Pre" were obtained from comparisons between sessions Pre -4 and Pre -3, Pre -3 and Pre -2, and Pre -2 and Pre -1. Similarly, data for "Early" were calculated from comparisons between Pre -1 and Rarr 1 and Rarr 1 and Rarr 2, and data for "Late" were derived from comparisons between Rarr 2 and Rarr 3, Rarr 3 and Rarr 4, and Rarr 4 and Rarr 5. The transition was quantified by determining the cell density at each bin to enable the comparison of transitions to different cell categories.

Data are expressed as mean \pm SEM. In both analysis of variance (ANOVA) and the Friedman test, *p*-values were adjusted for post hoc multiple comparisons. Exact *p*-values are presented unless *p* < 0.0001.

ACKNOWLEDGMENTS

This work was supported by Grants-in-Aid for Scientific Research from the Ministry of Education, Culture, Sports, Science and Technology (MEXT)/Japan Society for the Promotion of Science (JSPS) 25830023, 15H01571, 17H05695, 17K19633 and 19K16293 to K.M.; Grants-in-Aid for Scientific Research 26115504, 15H05723, 16H06536, the program for Brain Mapping by Integrated Neurotechnologies for Disease Studies (Brain/MINDS) from MEXT and the Japan Agency for Medical Research and Development (AMED) and Regional Innovation Cluster Program grant (City Area Type, Central Saitama Area) from MEXT to J.N.; RIKEN and Grants-in-Aid for Scientific Research 22110006, 16H01292 and 18H05434 to Y.H.; and Precursory Research for Embryonic Science and Technology (PRESTO) JPMJPR12A1 from the Japan Science and Technology Agency (JST) and Grants-in-Aid for Scientific Research 17H05985, 19H04942, 20H03550 and 20K21561 to M.S.

CONFLICT OF INTEREST

Y. H. was supported in part by Takeda Pharmaceutical Co. Ltd., Fujitsu Laboratories, and DWANGO.

DATA AVAILABILITY STATEMENT

The data that support the findings of this study are available from the corresponding author upon reasonable request.

ORCID

Kotaro Mizuta  <https://orcid.org/0000-0003-3369-8997>

Junichi Nakai  <https://orcid.org/0000-0001-9963-2603>

Yasunori Hayashi  <https://orcid.org/0000-0002-7560-3004>

Masaaki Sato  <https://orcid.org/0000-0002-5206-3375>

REFERENCES

- Bourboulou, R., Marti, G., Michon, F. X., El Feghaly, E., Nouguiet, M., Robbe, D., ... Epszstein, J. (2019). Dynamic control of hippocampal spatial coding resolution by local visual cues. *eLife*, 8, e44487.
- Dupret, D., O'Neill, J., Pleydell-Bouverie, B., & Csicsvari, J. (2010). The reorganization and reactivation of hippocampal maps predict spatial memory performance. *Nature Neuroscience*, 13, 995–1002.
- Gauthier, J. L., & Tank, D. W. (2018). A dedicated population for reward coding in the hippocampus. *Neuron*, 99, 179–193.e7.
- Hainmueller, T., & Bartos, M. (2018). Parallel emergence of stable and dynamic memory engrams in the hippocampus. *Nature*, 558, 292–296.
- Hetherington, P. A., & Shapiro, M. L. (1997). Hippocampal place fields are altered by the removal of single visual cues in a distance-dependent manner. *Behavioral Neuroscience*, 111, 20–34.
- Hollup, S. A., Molden, S., Donnett, J. G., Moser, M. B., & Moser, E. I. (2001). Accumulation of hippocampal place fields at the goal location in an annular watermaze task. *The Journal of Neuroscience*, 21, 1635–1644.
- Kobayashi, T., Nishijo, H., Fukuda, M., Bures, J., & Ono, T. (1997). Task-dependent representations in rat hippocampal place neurons. *Journal of Neurophysiology*, 78, 597–613.
- Mankin, E. A., Sparks, F. T., Slayyeh, B., Sutherland, R. J., Leutgeb, S., & Leutgeb, J. K. (2012). Neuronal code for extended time in the hippocampus. *Proceedings. National Academy of Sciences. United States of America*, 109, 19462–19467.
- O'Keefe, J., & Conway, D. H. (1978). Hippocampal place units in the freely moving rat: Why they fire where they fire. *Experimental Brain Research*, 31, 573–590.

- Rubin, A., Geva, N., Sheintuch, L., & Ziv, Y. (2015). Hippocampal ensemble dynamics timestamp events in long-term memory. *eLife*, 4, e12247.
- Sato, M., Kawano, M., Mizuta, K., Islam, T., Lee, M. G., & Hayashi, Y. (2017). Hippocampus-dependent goal localization by head-fixed mice in virtual reality. *eNeuro*, 4, ENEURO.0369-16.2017.
- Sato, M., Mizuta, K., Islam, T., Kawano, M., Sekine, Y., Takekawa, T., ... Hayashi, Y. (2020). Distinct mechanisms of over-representation of landmarks and rewards in the hippocampus. *Cell Reports*, 32, 107864.
- Wiener, S. I., Paul, C. A., & Eichenbaum, H. (1989). Spatial and behavioral correlates of hippocampal neuronal activity. *The Journal of Neuroscience*, 9, 2737-2763.
- Zaremba, J. D., Diamantopoulou, A., Danielson, N. B., Grosmark, A. D., Kaifosh, P. W., Bowler, J. C., ... Losonczy, A. (2017). Impaired hippocampal place cell dynamics in a mouse model of the 22q11.2 deletion. *Nature Neuroscience*, 20, 1612-1623.
- Ziv, Y., Burns, L. D., Cocker, E. D., Hamel, E. O., Ghosh, K. K., Kitch, L. J., ... Schnitzer, M. J. (2013). Long-term dynamics of CA1 hippocampal place codes. *Nature Neuroscience*, 16, 264-266.

SUPPORTING INFORMATION

Additional supporting information may be found online in the Supporting Information section at the end of this article.

How to cite this article: Mizuta K, Nakai J, Hayashi Y, Sato M. Multiple coordinated cellular dynamics mediate CA1 map plasticity. *Hippocampus*. 2021;31:235-243. <https://doi.org/10.1002/hipo.23300>